JOURNAL OF GEOPHYSICAL RESEARCH, VOL. 97, NO. D8, PAGES 7829–7840, MAY 30, 1992

Ultraviolet Radiation in the Arctic: The Impact of Potential Ozone Depletions and Cloud Effects

SI-CHEE TSAY

Universities Space Research Association, NASA/Goddard Space Flight Center, Greenbelt, Maryland

KNUT STAMNES

Geophysical Institute and Department of Physics, University of Alaska, Fairbanks

An atmospheric radiation model is used to study the combined effects of ozone depletions/redistributions and particulate clouds on atmospheric heating/photolysis rates and ultraviolet radiation reaching the biosphere. Four types of particulate clouds prevalent in the summertime Arctic are considered: stratospheric aerosols, tropospheric aerosols (Arctic haze), cirrus clouds, and stratus clouds. The effects of ozone depletion and vertical redistributions of ozone are also examined. The main findings are as follows: (1) stratus clouds provide significant protection from ultraviolet radiation exposure, but while stratospheric aerosols imply increased UVB exposure, Arctic haze results in a decrease; (2) a redistribution of ozone from the stratosphere to the troposphere tends to decrease UV exposure, but for low solar elevations an increase may occur; (3) a 20% ozone depletion leads to about 0.4 K/d cooling in the lower stratosphere, while redistribution of ozone from the stratosphere to the troposphere implies a warming of about 0.015 K/d in the upper troposphere; (4) stratus clouds may cause a large warming in the middle and upper stratosphere (0.8 K/d); (5) clouds have little effect on ozone photolysis leading to $O(^1D)$ production at altitudes higher than 25 km; (6) for ozone photolysis leading to $O(^3P)$ production photolysis rates may increase by 50% or more throughout the atmosphere due to multiple scattering by stratus clouds.

1. Introduction

Ever since *Farman et al.* [1985] reported a substantial (almost 50%) reduction in column ozone abundance during the previous decade over Halley Bay, Antarctica, and suggested that chlorine-containing compounds could be causing the observed depletion, the possibility of significant ozone loss over the polar regions resulting from anthropogenic emissions of chlorofluorocarbons has been a matter of considerable concern. The temporal and spatial evolution of this so-called "ozone hole" occurring over Antarctica during austral spring has since been closely monitored by ground-based as well as space-borne instruments. Although no depletions of a similar magnitude have yet been reported in the Arctic, recent data from the Airborne Arctic Stratospheric Experiment (AASE) suggest that the Arctic stratosphere is chemically primed for ozone destruction and that depletions as large as 20% may have occurred inside the northern polar vortex [*Brune*, 1990; *Proffitt et al.*, 1990]. First results from the AASE experiment were recently published in a special issue of *Geophysical Research Letters* (volume 17, number 4, 1990). Indications of Arctic ozone depletions were also inferred from balloon data taken during 1989. These data suggest that an ozone depletion took place over Kiruna, Sweden (68° N), in late January at an altitude of 22-26 km [*Hoffmann et al.*, 1989], and over Alert, Canada (82° N), from January 24 to February 22 at an altitude of 18-24 km [*Evans*, 1990]. Moreover, the Ozone Trends Panel World Meteorological Organization (WMO), 1988] found that a comparison of total column ozone data from 1979-1980 with 1986-1987 indicated a decrease of 4-10% between 65° and 80° N during the period from November to February.

One consequence of the formation of "holes" in the Arctic ozone shield would be reduced stratospheric heating due to less ozone absorption of solar ultraviolet radiation. This reduced heating may in turn lead to significant alteration in stratospheric circulation. Another consequence which has caused widespread public concern, especially in the populated regions of northern Europe and Scandinavia, is the expected increase in harmful ultraviolet radiation reaching the biosphere as a result of an ozone depletion. Measurements under the "ozone hole" in Antarctica have clearly shown that enhanced levels of biologically relevant ultraviolet radiation are directly linked to the observed decrease in ozone abundance [e.g., *Lubin et al.*, 1989; *Stamnes et al.*, 1990]. These measurements also demonstrate that clouds have a profound effect on ultraviolet penetration.

The strong interaction of radiation with ozone and clouds as well as the natural (including biogenic) and anthropogenic origin of cloud condensation nuclei and trace gases important in the ozone chemistry provide a tight coupling between the stratosphere, the troposphere, the biosphere and human activities. Variations in stratospheric ozone will modify the amount of solar ultraviolet radiation available for absorption in the atmosphere and at the surface. Such modifications may in turn lead to changes in (1) atmospheric composition through altered photochemistry, (2) circulation through changes in warming/cooling rate profiles, and (3) terrestrial ecosystems through modulations in biologically effective ultraviolet radiation reaching the biosphere. Similar effects may result from redistributions of ozone from the stratosphere to the troposphere, caused by depletions in the stratosphere due to

Paper number 91JD02915.
0148-0227/92/91JD-02915$05.00

natural or anthropogenic processes, and/or enhancements in the troposphere due to industrial pollution. The response of the atmosphere-biosphere system to such photochemical, dynamical and radiative forcings is not well understood at present, but deserves careful consideration. One necessary step towards a better understanding of this coupled system is an improved knowledge of the radiation field which determines atmospheric warming/cooling and photolysis rates as well as biological UV doses. An assessment of the sensitivity of these quantities to the changes in atmospheric composition is also essential.

One of the least understood components of this coupled system is the radiative effects of particulate clouds, as well as the environmental conditions leading to their formation and dissipation. To some extent, problems related to the effects of solar elevation, surface albedo and cloud parameters such as optical depth, altitude and cloud fraction on ozone absorption have been studied by previous investigators. For example, *Shettle and Green* [1974] examined the sensitivity of transmitted ultraviolet radiation to variations in solar elevation, ozone abundance, aerosol optical depths, surface albedo, and ground height above sea level. *Luther and Gelinas* [1976] and *Nicolet et al.* [1982] considered the effects of molecular multiple scattering and surface albedo on photodissociation rates as compared to absorption only of the direct solar beam. Stratified clouds were considered by *Spinhirne and Green* [1978], who found that absorption by tropospheric ozone renders the penetration of ultraviolet radiation of wavelengths shorter than 300 nm sensitive to cloud height and surface albedo, whereas for wavelengths longer than 300 nm penetration depends mostly on cloud optical depth. This was confirmed by *Thompson* [1984], who considered photochemical production of ozone in an unpolluted troposphere. The effects of clouds on tropospheric photolysis rates were also studied by *Madronich* [1987]. More recently, *Frederick and Snell* [1990] analyzed data obtained from the Robertson-Berger meter network and concluded that at some locations the variations in erythemal dose due to alterations in cloudiness could be comparable to that resulting from trends in total column ozone.

In this paper we focus specifically on the combined effects of clouds and ozone on atmospheric warming and photolysis rates in the Arctic environment as well as on the penetration of ultraviolet radiation into the biosphere. In section 2 we introduce four types of particulate clouds that are often observed in the summertime Arctic. The physical properties of these clouds are constrained by available observations and the spectral dependence of their optical characteristics are inferred from computations assuming spherical particles. In section 3 we discuss the particular ozone depletion scenario adopted in

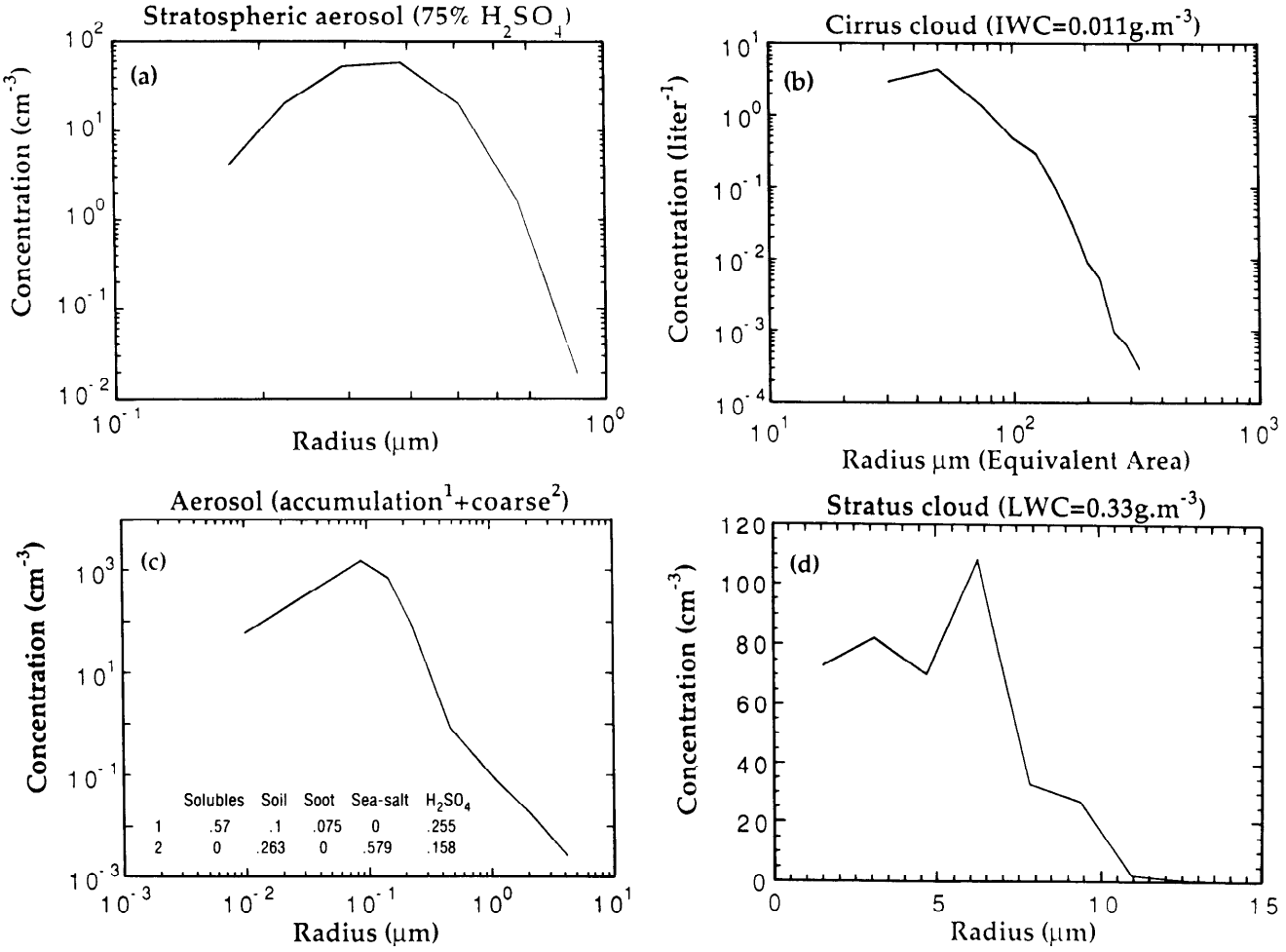

Fig. 1. Size distributions of (*a*) the stratospheric aerosols, (*b*) the cirrus clouds, (*c*) the arctic haze, and (*d*) the arctic stratus clouds used in Mie computations (see text for details).

the present study including two ozone profiles in which the ozone is redistributed from the stratosphere to the troposphere in such a way that the total column content is kept constant. The spectral resolution utilized in the computations as well the radiative transfer model is also described in section 3. Our results are provided in section 4, where we present and discuss biological UV dose as well as atmospheric warming and photolysis rates for various combinations of ozone depletions and cloud conditions. A summary of this study is provided in section 5.

2. Particulate Cloud Models

We have considered four types of particulate clouds in this study: stratospheric aerosols, cirrus clouds (ice crystals), arctic haze, and arctic stratus clouds (water droplets). Optical properties (i.e., extinction, scattering coefficient, and phase function) can be obtained by solving Maxwell equations if the cloud physical characteristics (such as size, shape, chemical composition) are specified. However, due to (1) limited knowledge of the actual shapes of particulate matter in the atmosphere, (2) limited availability of numerical algorithms valid for nonspherical shapes, and (3) limited computer resources available to us, we shall in this study consider spherical shapes or "equivalent" spherical particles. The precise meaning of equivalent will be defined below. We will apply well-known solutions to the problem of scattering of radiation by a dielectric sphere (the so-called Mie theory) to compute the optical properties of these particles. Therefore, the size distributions and the refractive indices of the model clouds are the only input parameters required in the computations to obtain single scattering properties of the cloud particles. Due to the scarcity of relevant observations we shall use these two parameters to define a mean state of the cloud and hence to provide a convenient approximation to the complex nature of clouds.

2.1. *Stratospheric Aerosols*

The role of stratospheric aerosols in modifying the propagation of atmospheric radiation has been the subject of numerous climate-related investigations. Obtaining in situ information on particle size and composition is difficult, due to the instrumental inaccessibility to the high altitudes involved, and the large dynamic size range. *King et al.* [1984] synthesized the available information on stratospheric aerosols and combined it with physical models to infer that the stratospheric aerosols after the El Chichon eruption consisted primarily of spherical liquid droplets having a 75% concentration by weight of sulfuric acid and a typical size distribution as shown in Figure 1*a*. We have adopted this aerosol model to compute the wavelength dependence of aerosol optical properties and we have constrained the modeled optical depth to lie between 0.15 and 0.25 in agreement with available observations.

2.2. *Cirrus Clouds*

Ice crystal clouds constitute an ambiguous puzzle, partly due to the difficulty involved in obtaining in situ observations within cirrus clouds and partly because of their characteristics, such as habits, which depend on environmental conditions. *Stackhouse and Stephens* [1991] report on an attempt to analyze recent observations of physical and radiative properties of cirrus clouds (i.e., the First ISCCP Regional Experiment Intensive Field Observation). They used the measured distributions of maximum crystal size and cross-sectional area [*Heymsfield et al.*, 1990] to construct an effective size distribution consisting of equivalent spherical particles with the same cross-sectional area. This spherical size distribution (with equivalent cross-sectional area) led to significantly better agreement between observed and computed radiative fluxes than a distribution based on equivalent radius. Figure 1b shows the crystal size distribution of equivalent area "spheres" with observed ice water content of 0.011 g m^{-3} adopted in this study from *Stackhouse and Stephens* [1991]. The optical depth for our cirrus cloud model is taken to be 1.2, which is close to the bulk of the observed values.

2.3. *Arctic Haze*

Arctic haze has been reported since the 1950s. An important feature of arctic haze is that it contains a substantial amount of anthropogenic compounds such as sulfur elements and graphitic particles. Based on available observations, *Blanchet and List* [1983] constructed a sophisticated physical model to represent the mean state of springtime arctic haze, and their simulated scattering properties agreed very well with those measured by *Heintzenberg* [1980]. Figure 1*c* shows the measured size distribution which has a strong accumulation mode peaking at about 0.1μm and a weak coarse mode peaking at about 0.5μm. Each mode is composed of different chemical species with dry mass fractions indicated in the inset of Figure 1*c*. This haze model allows for particle coating (e.g., two concentric spheres of insoluble core covered by sulphuric acid) and mixing (i.e., external and internal) as well as growth depending on available water vapor. These features, in turn, are expected to alleviate somewhat the assumption of sphericity in shape. The concentrations of arctic haze in summertime are far less than those in springtime, and we have limited the spectral optical depth to lie between 0.05 and 0.15, which is consistent with available observations [e.g., *Shaw*, 1982].

2.4. *Arctic Stratus Clouds*

Another important feature in the summertime Arctic is the persistent occurrence of extensive layers of stratus clouds. Using data from the Arctic Stratus Clouds Experiment conducted over the Beaufort Sea in June 1980, *Tsay and Jayaweera* [1984] documented the physical characteristics of these stratiform clouds. Summertime arctic stratus clouds consist mainly of spherical water droplets. *Tsay and Jayaweera* [1984] found that the liquid water content generally increased with height inside the cloud, as a result of an increase in drop size rather than concentration. The drop size distribution near the base was monomodal, characteristic of condensation on a nucleus spectrum, but changed to bimodal near the cloud top perhaps due to mixing of dry air entrained from above. We have adopted a size distribution, as shown in Figure 1*d*, obtained at the middle of a relatively thick cloud layer to represent the mean state of arctic stratus clouds. This particular cloud had a liquid water content of 0.33 g m^{-3}, and a corresponding optical depth of about 36 in the ultraviolet-visible part of the spectrum.

3. Atmospheric Radiation Model

3.1. *Atmospheric Profiles and Boundary Conditions*

In the following model simulations, we adopted the pressure and ozone density profiles of the sub-Arctic summer

atmosphere from the compilation of *McClatchey et al.* [1972]. The pressure dependence is used to compute the column density of air required to determine the molecular (Rayleigh) scattering. In the spectral range of interest here, absorption by trace gases other than ozone is relatively unimportant. Figure 2 shows the ozone vertical distribution (solid curve) with a total column content of 350 DU (Dobson unit) and about 10% of this amount (34 DU) contained in the troposphere.

Satellite-based (such as NASA/Total Ozone Mapping Spectrometer (TOMS) and NOAA/Tiros Operational Vertical Sounder (TOVS)) and ground-based (Dobson network) ozone measurements have been used to estimate global trends in ozone abundance [e.g., *WMO*, 1988]. A recent reevaluation of the TOMS (version-6) gridded data base suggests a 4%-6% per decade decrease in ozone abundance in the Arctic during the last decade for the summer months [*Stolarski et al.*, 1990]. However, it is commonly found that daily variations in total column ozone content can frequently be as high as 20% in the summertime Arctic [*Chesters and Krueger*, 1989]. For demonstration purposes, we have chosen a somewhat extreme 20% depletion scenario in this study which is shown in Figure 2 as the dash-dotted (280 DU) curve mimicking the shape of the antarctic ozone depletions [e.g., *Solomon*, 1988]. To examine the impact of increasing the tropospheric ozone content at the expense of the stratospheric component, two additional profiles are shown in Figure 2: the dashed curve was obtained by redistributing ozone from the stratosphere to the troposphere in the original sub-Arctic summer profile, while the dotted curve corresponds to a similar redistribution for the depleted curve. It should be noted that the total column ozone abundance was constrained to be unaffected by this redistribution. It has been reported [*Bruhl and Crutzen*, 1989 and references therein] that the summertime tropospheric ozone in Europe has increased by about 60% from 1967 to 1982. We have increased the tropospheric ozone by about 50% (about 15 DU) in the two redistribution profiles shown in Figure 2 (total 50 DU for the dashed curve and 48 DU for the dotted curve in the troposphere).

A surface albedo of 0.2 was used in the present computations, corresponding to an averaged albedo of tundra or continental vegetation [*Kondratyev*, 1969]. For simplicity, the wavelength dependence of the surface albedo is neglected in our model computations. The extraterrestrial solar flux is adopted from the recent compilation of *Nicolet* [1989] and solar zenith angles of 55° and 75°, respectively, are used to represent the high and low sun elevations in the summertime Arctic.

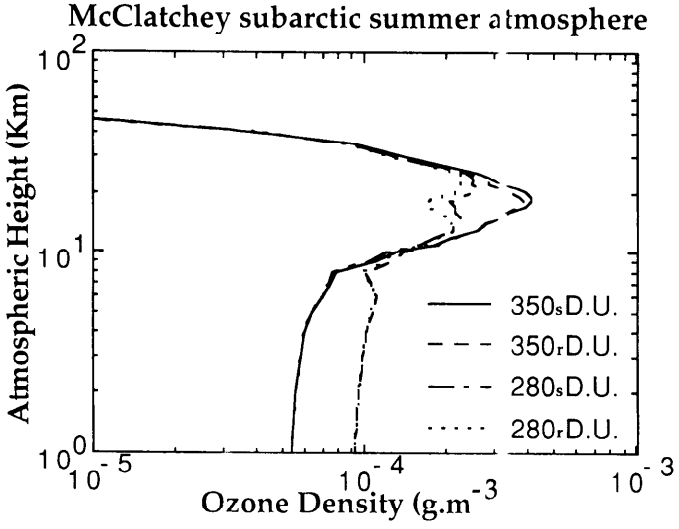

Fig. 2. Ozone density profile for the McClatchey sub-Arctic summer atmosphere adopted in this study.

3.2. *Spectral Resolution*

We have adopted the absorption cross-section of ozone and molecular oxygen, as shown in Figure 3, together with the extraterrestrial solar flux in 1 nm resolution [cf. *Stamnes and Tsay*, 1990 and references therein]. For convenience in characterizing the spectral absorption, the spectral range between 175 nm and 700 nm considered in this study was divided into four spectral regions. In region 1 (175-290 nm) there is an ozone absorption peak, overlapping with absorption by molecular oxygen. In region 2 ranging from 290 nm to 315 nm (UVB) ozone absorption decreases rapidly with wavelength. Region 3 covers the UVA spectral range between 315 nm and 400 nm. In region 4 (400-700 nm), the relatively weak ozone absorption in the Chappuis band occurs. *Stamnes and Tsay* [1990] have discussed the spectral resolution required to obtain adequate accuracy in computations of UV dose, atmospheric warming and photolysis rates. In this paper, we have been quite conservative and adopted a resolution

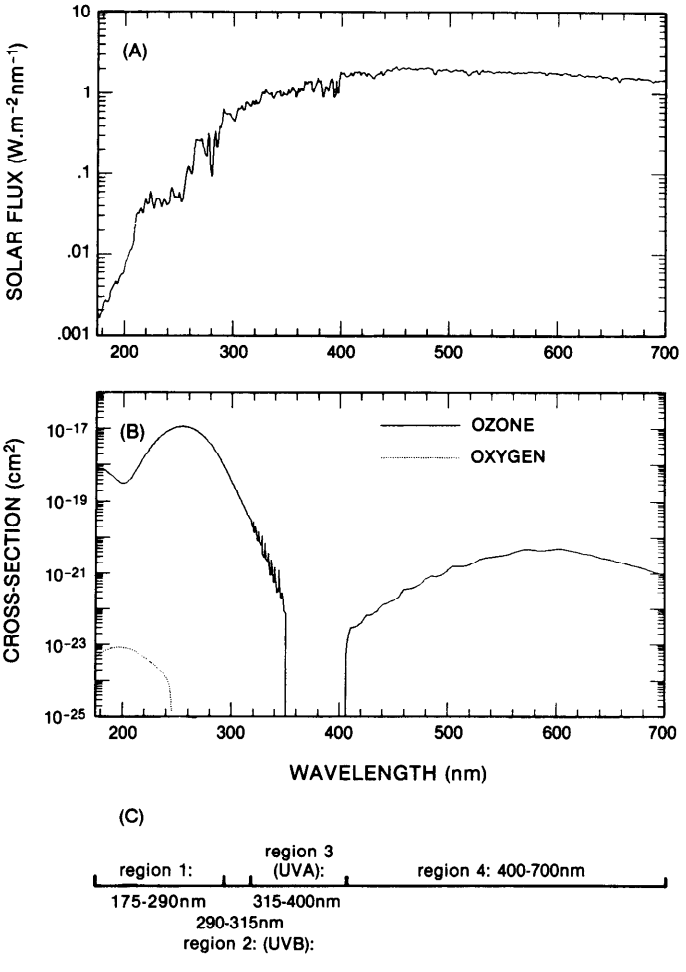

Fig. 3. Spectral characteristics of (*a*) solar flux at the top of the atmosphere, (*b*) absorption cross sections for molecular oxygen (dotted line) and ozone (solid line), and (*c*) band regions considered in this study.

of 1 nm for the UV dose calculation and 5 nm resolution for the computation of atmospheric warming and photolysis rates.

3.3. *Radiative Transfer*

UV radiation penetrating to the surface and to various levels in the atmosphere contains both direct and diffuse components [*Chandrasekhar*, 1960]. The direct radiation is simply exponentially attenuated upon passage through the atmosphere, while the diffuse component requires solutions of the radiative transfer equation including the effects of multiple scattering. *Henriksen et al.* [1989] demonstrated clearly from the measurements in the summertime Arctic that the diffuse component dominate the total (diffuse plus direct) ultraviolet radiation at the surface. Although many numerical radiative transfer models have appeared in the literature, in this study we have adopted a recent implementation of the discrete ordinate method valid for vertically inhomogeneous, nonisothermal, plane-parallel media [*Stamnes et al.*, 1988] because of its computational efficiency and reliability. *Tsay et al.* [1990] provided a comprehensive validation of the algorithm and a demonstration of its versatility. Direct application of this method can be found in *Tsay et al.* [1989] and *Stamnes and Tsay* [1990]. For large solar zenith angles spherical geometry will in general be required. But to compute mean intensities for solar zenith angles less than 90°, it is sufficient to compute the direct beam attenuation correctly using spherical geometry and then use plane geometry in the multiple scattering calculations [*Dahlback and Stamnes*, 1991]. In the present study we have used plane-parallel geometry, which is adequate for the solar zenith angles (75° and less) considered.

We have treated absorption by ozone and molecular oxygen, scattering by air molecules (Rayleigh) as well as scattering and absorption by particulate clouds in the model. Figure 4 shows the vertical structure of model atmospheres consisting of four different "cloud" layers embedded in a background clear sky atmosphere as follows: a stratospheric aerosol layer between 13 km and 23 km, a cirrus cloud layer between 5 km and 8 km, an arctic haze layer between 2 km and 4 km, and a stratus cloud layer between 1 km and 1.5 km. The physical properties of these particulate clouds are constrained by available observations. When an atmospheric layer contains a mixture of gas molecules and particulate clouds, effective optical properties are obtained by using weighted averages [e.g., *Tsay et al.*, 1989].

The computation of atmospheric warming rate requires the determination of the divergence of the net flux, which is proportional to the mean intensity [cf. *Stamnes*, 1986]. In fact, as discussed by *Stamnes and Tsay* [1990], biological UV dose and atmospheric warming and photolysis rates are all proportional to the mean intensity which is obtained by solving the radiative transfer equation [cf. *Stamnes et al.*, 1988 for details]. Here we follow very closely the procedures for spectral averaging and integration presented by *Stamnes and Tsay* [1990] for computation of biological UV dose, atmospheric warming and photolysis rates.

4. Results and Discussion

4.1. *Biological UV Dose Rates*

The biological effect of ultraviolet radiation can be conveniently expressed in terms of the UV dose rate defined as a convolution of a biological action spectrum with the irradiance spectrum. The actual UV dose is then obtained by integrating the dose rate over the time of exposure. Four different types of action spectra [*Stamnes and Tsay*, 1990 and references therein] are shown in Figure 5: a generalized DNA damage spectrum, a generalized plant damage spectrum, an action spectrum for erythema, and a response spectrum for the Robertson-Berger meter designed to approximate the erythema response of Caucasian skin. The major response of these four biological action spectra occurs in the UVB region with a rapid decrease in the UVA spectral range. In the present study we have arbitrarily chosen the action spectrum of erythema for demonstration purposes. It should be noted, however, that use of a different action spectrum would lead to qualitatively similar results.

Table 1 shows the variation in UV dose rate for erythema under various cloud and ozone scenarios. The results are presented as deviations in percent from the standard case with clear sky and unperturbed ozone content. Computations for two spectral regions are shown: UVB only and UVB plus UVA. Substantial increase in UVB dose rate occurs as a consequence of an ozone depletion. The addition of UVA makes the damage incurred by an ozone depletion appear much less severe in

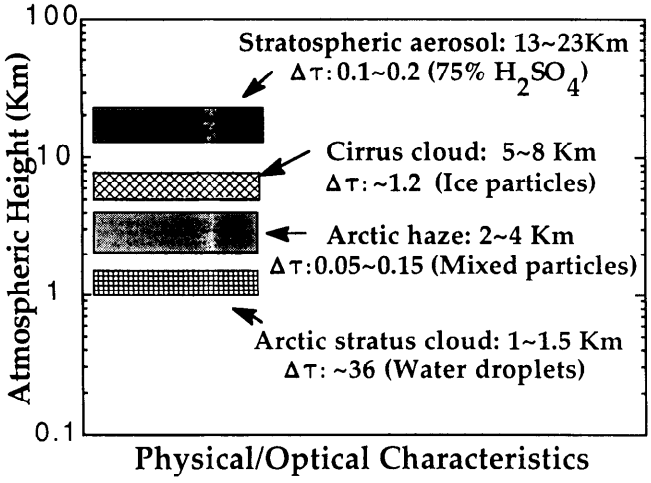

Fig. 4. Illustration of the physical and optical characteristics of four types of particulate clouds embedded in the model atmospheres.

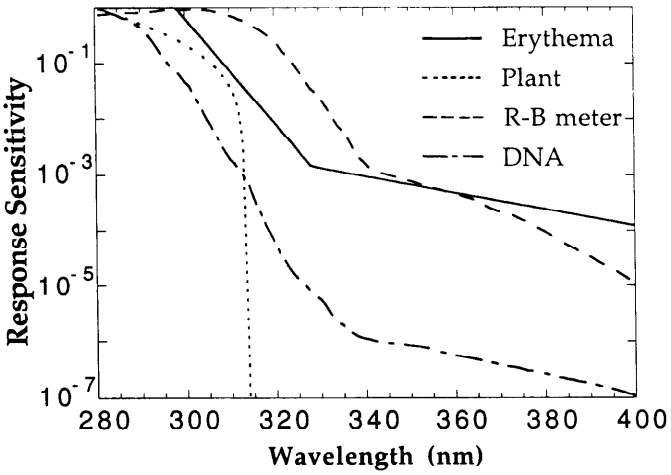

Fig. 5. Action spectra used to compute UV dose rates for several biological responses.

TABLE 1. Variation of UV Dose Rates for Erythema in the Sub-Arctic Summer Atmosphere, Under Various Cloud Conditions

290-400 nm (UVA+UVB)										
	(*a*) Zenith angle 55°					(*b*) Zenith angle 75°				
DU	Clear	H_2SO_4	Cirrus	Haze	Stratus	Clear	H_2SO_4	Cirrus	Haze	Stratus
^{1}350s	0%	-6%	-12%	-5%	-71%	0%	-8%	-23%	-9%	-75%
^{2}350r	-2%	-7%	-14%	-6%	-72%	0%	-7%	-22%	-9%	-75%
^{3}280s	27%	20%	12%	21%	-63%	19%	11%	-6%	9%	-69%
^{4}280r	24%	17%	9%	18%	-64%	20%	11%	-6%	10%	-69%
290-315 nm (UVB)										
	(*c*) Zenith angle 55°					(*d*) Zenith angle 75°				
DU	Clear	H_2SO_4	Cirrus	Haze	Stratus	Clear	H_2SO_4	Cirrus	Haze	Stratus
^{1}350s	0%	-6%	-12%	-5%	-70%	0%	3%	-13%	-6%	-70%
^{2}350r	-3%	-9%	-15%	-8%	-72%	1%	5%	-12%	-5%	-70%
^{3}280s	48%	38%	30%	41%	-56%	64%	65%	42%	54%	-50%
^{4}280r	43%	34%	25%	36%	-58%	67%	68%	45%	56%	-50%

Note: Clear stands for clear sky; H_2SO_4 for stratospheric aerosol, Cirrus for cirrus cloud; Haze for arctic haze; Stratus for arctic stratus cloud. Subscript s/r is for standard/redistribution profile.

^{1}350DU ozone in total column amount (cf. solid curve in Figure 2),
^{2}Same as in footnote 1, but with a ~50% increase in the troposphere and a corresponding depletion in the stratosphere (cf. dashed curve in Figure 2),
^{3}280DU or a 20% depletion of ozone in footnote 1 (cf. dashed-dotted curve in Figure 2),
^{4}Same as in footnote 3, but with a ~50% increase in the troposphere and a corresponding depletion in the stratosphere (cf. dotted curve in Figure 2).

agreement with previous findings [e.g., *Dahlback et al.*, 1989].

Of the different clouds considered here the low-level stratus cloud provides the best shield from UV exposure, because strong scattering and enhanced photon path lengths inside the cloud lead to both increased reflection and enhanced absorption by ozone. The changes in ozone profiles considered here have no significant impact in the presence of a thick stratus cloud, especially for the case of 75° solar zenith angle which implies a doubling of the air mass compared to 55° solar zenith angle. When the cloud optical depth is moderate, the variation in biological UV dose rates shows relatively stronger dependence on optical depth (e.g., cirrus cloud compared to stratospheric aerosol/arctic haze) than on altitude and optical characteristics, such as high altitude, nonabsorbing stratospheric aerosol in comparison to arctic haze. We note also that the stratospheric aerosol and the (tropospheric) arctic haze have very similar effects on the UV dose rate when the spectral range from 290 nm to 400 nm is used. But when the integration extends over the UVB range only the non-absorbing stratospheric aerosol may lead to an increase in UV dose for large solar zenith angles, while tropospheric aerosols (arctic haze) result in a decrease (cf. Table 1).

It has been shown previously [e.g., *Bruhl and Crutzen*, 1989; *Frederick et al.*, 1989] that an increase in tropospheric ozone content as well as enhanced abundances of other absorbing gases and particulates may lead to a decrease (rather than an increase) in biological UV dose when the total ozone column is depleted. It is quite clear from Tables 1*a* and 1*c* (solar zenith angle 55°) that a redistribution of ozone from the stratosphere to the troposphere tends to decrease the biologically effective ultraviolet radiation. Depending on atmospheric conditions this decrease ranges from 1% up to 5%. However, when the solar zenith angle increases to 75°, the UV dose rate may actually increase by as much as 3% in the UVB region. Stratospheric ozone depletion leads to more ultraviolet radiation (both direct and diffuse) in the troposphere. A redistribution of ozone in which the column content stays fixed does not, however, affect the penetration of direct radiation to the surface, because the total optical depth is unchanged. Thus when the sun is low and multiple scattering important, the diffuse radiation at the surface may increase with a redistribution of ozone from the stratosphere to the troposphere, while the direct beam radiation remains unchanged. A detailed explanation for this zenith angle dependence is provided below.

The source of the diffuse radiation is the direct beam attenuated radiation which at any level is proportional to $\exp(-\tau/\mu_0)$, where τ is the vertical optical depth (defined to be zero at the top of the atmosphere) and μ_0 the cosine of the solar zenith angle. If the stratospheric optical depth decreases by an amount $\delta\tau$ as a result of an ozone depletion, then the relative enhancement in direct beam radiation reaching the troposphere is $(\exp[\delta\tau/\mu_0]-1)$. This shows that the relative enhancement increases rapidly with increasing solar zenith angle (decreasing μ_0). Thus for a redistribution of ozone from the stratosphere to the troposphere the fate of the diffuse radiation in the troposphere and at the surface depends on two competing factors: (1) increased absorption by tropospheric ozone due to increased path lengths of photons in the troposphere, and (2) enhancement of the source of diffuse radiation in the troposphere due to an increase in the direct beam radiation passing through the stratosphere. The first factor will lead to a decrease in diffuse radiation at the surface; the second one to an increase. The latter is strongly dependent on solar zenith angle, while the former is not. This explains why factor (1) dominate for small solar zenith angles (leading to a decrease in UV dose), and factor (2) for larger solar zenith angles implying an enhancement in diffuse ultraviolet radiation reaching the surface and therefore in UV dose.

The percent increase in UV dose per percent decrease in ozone abundance is defined as the amplification factor. For clear sky conditions and a 20% ozone depletion, the amplification factor ranges from 1.35 to 0.95 (decreasing with increasing solar zenith angle) for the 290-400 nm spectral region, and from 2.4 to 3.2 (increasing with increasing solar

zenith angle) for the UVB band only. This shows that the particular type of biological response determines the amplification factor. Thus, an action spectrum with most of the response in the UVB spectral region and little in the UVA region (e.g., the generalized action spectrum for plants shown in Figure 5), will have a large amplification factor that will generally increase with increasing solar zenith angle, while an action spectrum with a significant tail in the UVA region (e.g., that for erythema), will have a smaller amplification factor that will tend to decrease with increasing solar zenith angle. When particulate clouds are considered, it becomes more complicated, due to the strong influence by the optical depth.

4.2. *Atmospheric Warming Rates*

The computations of atmospheric warming rates are performed for the spectral interval 175-700 nm, which covers the Hartley and Huggins bands in the ultraviolet and the Chappuis band in the visible part of the spectrum. These bands give rise to the major portion of the solar heating by ozone. A precise definition of the warming rates, as shown in Figure 6, is given by *Stamnes and Tsay* [1990], who also argue that warming rate is a better term for the time rate of change of temperature than heating rate which implies units of energy per unit time. Also, for convenience the unit of time is presented by per day which is a direct conversion from per second.

We start by showing in Figure 6*a* atmospheric warming rates for clear sky and 55° solar zenith angle. A 20% ozone depletion results in a maximum decrease in the warming rate of about 0.4 K/d in the lower stratosphere, and redistributions in ozone column content leads to a maximum increase in the warming rate of about 0.015 K/d in the upper troposphere. For 75° solar zenith angle these rates decrease to about 0.3 K/d and 0.01K/d, respectively. Changes in solar elevation do not alter the basic structure of the heating profiles in the depletion/redistribution scenarios considered here, but the magnitude becomes smaller for larger solar zenith angles. In the middle mesosphere, however, we probably have overestimated the warming rate, due to the coarse grid resolution available in the upper part of the McClatchey atmospheres (5-30 km grid above 25 km height and 1 km below). The common warming rate dip at about 80km [e.g., *Strobel*, 1978; *Brasseur and Solomon*, 1984] is not so pronounced in Figure 6*a*.

There is strong coupling in the stratosphere between the radiation, chemistry and dynamics. Changes in ozone content may perturb the balance of radiative energy between the absorption of solar radiation (mainly in the ultraviolet and in the visible Chappuis bands) and the emission of terrestrial radiation (i.e., the 9.6 μm band) and thereby alter the atmospheric temperature structure. This alteration in temperature, if any, will in turn influence ozone chemistry through changes in air density and via temperature dependent reaction rates as discussed by *Penner and Luther* [1981]. In addition, the dynamical structure of the atmosphere responds to and may be modified by these temperature fluctuations [e.g., *Fels et al.*, 1980; *Kiehl and Boville*, 1988] which are initiated by radiative perturbations. If the state of the atmosphere is changed due to the aforementioned mechanisms, one of the least understood ramifications of such changes is the impact of particulate clouds on the radiative heating/cooling. Moreover, the formation and dissipation of such clouds are strongly influenced by dynamical transport of aerosols, cloud condensation nuclei and water vapor. Therefore, to close this system the inclusion of infrared thermal effects is needed (cf. *WMO* [1988, 1989] for review). In this study, however, we limit the discussion to heating by ozone absorption in ultraviolet and visible part of the spectrum.

Figure 6*b* shows the difference in warming rates due to the effects of the four types of particulate clouds considered here with respect to the reference warming rate profile pertinent for the clear sky standard case with an ozone content of 350 DU. There is a large increase in radiative heating occurring in the middle and upper stratosphere (about 0.8 K/d) caused by the strong backscattering of solar radiation by the low-level stratus cloud. Similar results were also found in the studies by *Lacis and Hansen* [1974] and *Edwards* [1982], in which effective albedos were used instead of detailed microphysical models of the particulate clouds in their computations. This heating decreases with decreasing optical depth, except for the spike in the lower troposphere which is caused by absorption of radiation within the arctic haze layer.

The mid-stratosphere photochemical equilibrium zone is sensitive to the local temperature fluctuations [e.g., *Penner and Luther*, 1981] and to some extent the natural variations in ozone amount in the lower stratosphere and troposphere are determined by the transport of ozone downward from this region. One immediate question arises: To what extent may the particulate clouds act to offset perturbations in solar energy absorption caused by ozone depletions? In Figures 6*c*-6*f* we show the differences in the warming rate profiles (as compared to the clear sky standard case) for the four types of particulate clouds and the various ozone profiles adopted here. The common feature in these figures is the reduced warming of about 0.3-0.4 K/d in the lower stratosphere regardless of cloud type when a 20% ozone depletion occurs (dotted curve). In the middle and upper stratosphere the situation is different: the changes in the warming rate profiles for an ozone depletion vary in sign with cloud type. There is less heating for stratospheric aerosol and arctic haze; more heating for cirrus and stratus clouds; and the magnitude of the heating depends on cloud optical depth. The redistributions of less than 15 DU of ozone form the stratosphere to the troposphere (short-dashed and dash-dotted curves) lead to an increase in the warming of a few hundredths K/d in the troposphere, except within the absorbing arctic haze layer.

To construct a first-order picture of the effects of cloudiness on the radiative heating, clouds are often considered as plane-parallel. For broken clouds it has been customary to use an ensemble averaged radiation field consisting of a linear combination of clear sky and cloudy conditions, which may not be very realistic in most cases as pointed out by *Stephens* [1988]. Arctic stratus clouds are perhaps an exception to this situation in that they tend to be stratified into extensive layers which makes the plane-parallel assumption more justifiable. When the stratospheric ozone content is depleted by 20% as depicted in Figure 2, we estimate that an increase in cloudiness of about 20% for arctic stratus (or about 70% for cirrus) would be required to offset the temperature perturbations due to solar radiation in the mid-stratosphere. This estimate was arrived at by linearly weighting the clear sky (-0.15 K/d) and cloudy (+0.6 K/d) warming rates with the cloud amounts. Thus, the enhanced heating in the troposphere and the decreased heating in the lower stratosphere caused by the ozone depletion can not be counteracted by the clouds considered in this study.

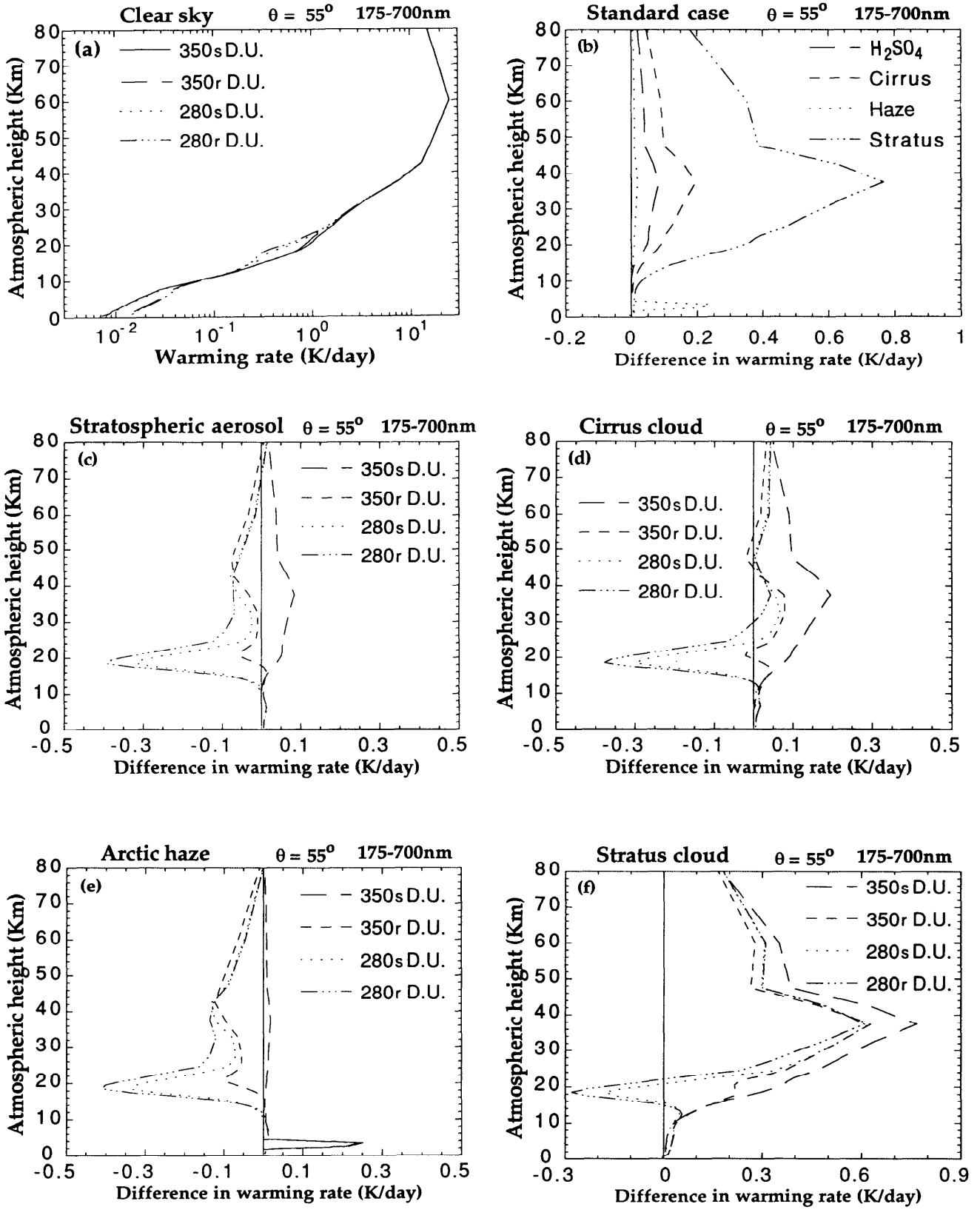

Fig. 6. Computed profiles of (*a*) clear sky warming rates for different ozone depletion scenarios, (*b*) difference in warming rates due to the introduction of particulate clouds into standard atmosphere of 350 DU ozone amount; and differences in warming rates in various ozone scenarios due to (*c*) stratospheric aerosols, (*d*) cirrus clouds, (*e*) arctic haze, and (*f*) arctic stratus clouds.

Therefore, an imbalance of the atmospheric radiative heating by solar radiation is very likely to be the result of these types of ozone depletions. To achieve a better understanding of this problem we must consider the coupled processes of dynamics, chemistry and radiation including the thermal infrared effects not considered in this study.

4.3. *Photolysis Rates*

Since detailed photochemical studies of ozone and other atmospheric constituents are not the main focus of this study, we shall limit ourselves to consider only photodissociation of ozone to demonstrate the impact that clouds might have on photolysis rates. In this computation we have for convenience assumed the quantum efficiency to be unity, and we have neglected the temperature dependence of the ozone photoabsorption cross section. In the spectral interval of interest here we used 315 nm as a demarcation line between ozone photolysis leading to $O(^3P)$ or $O(^1D)$ in agreement with theoretical predictions [e.g., *Brasseur and Solomon*, 1984]. Thus, for wavelengths longer than 315 nm in the Huggins and Chappuis bands the production of $O(^3P)$ occurs as a result of ozone photolysis, while $O(^1D)$ is produced for wavelengths shorter than 315 nm (i.e., Hartley bands).

The shapes of the photolysis rate profiles for a given spectral range and a specific solar zenith angle are similar for the four different ozone profiles. We first examine the standard case of 350 DU, as shown in Figures 7*a-d*, to delineate the effects of different types of clouds on the photolysis rates. For the spectral region 175-315 nm there is virtually no effect caused by the existence of clouds on photolysis rates at altitudes higher than 25 km due to the saturation of ozone absorption for these short wavelengths. Notable increases in photolysis rates by stratus are evident in the troposphere, caused by absorption due to multiple scattering occurring at wavelengths in the longward tail of the UVB spectral range. When the sun gets lower in the sky (Figure 7*c*) the general picture remains unchanged, but the rates are about one order of magnitude smaller in the troposphere, due to the increased photon path length through the atmosphere.

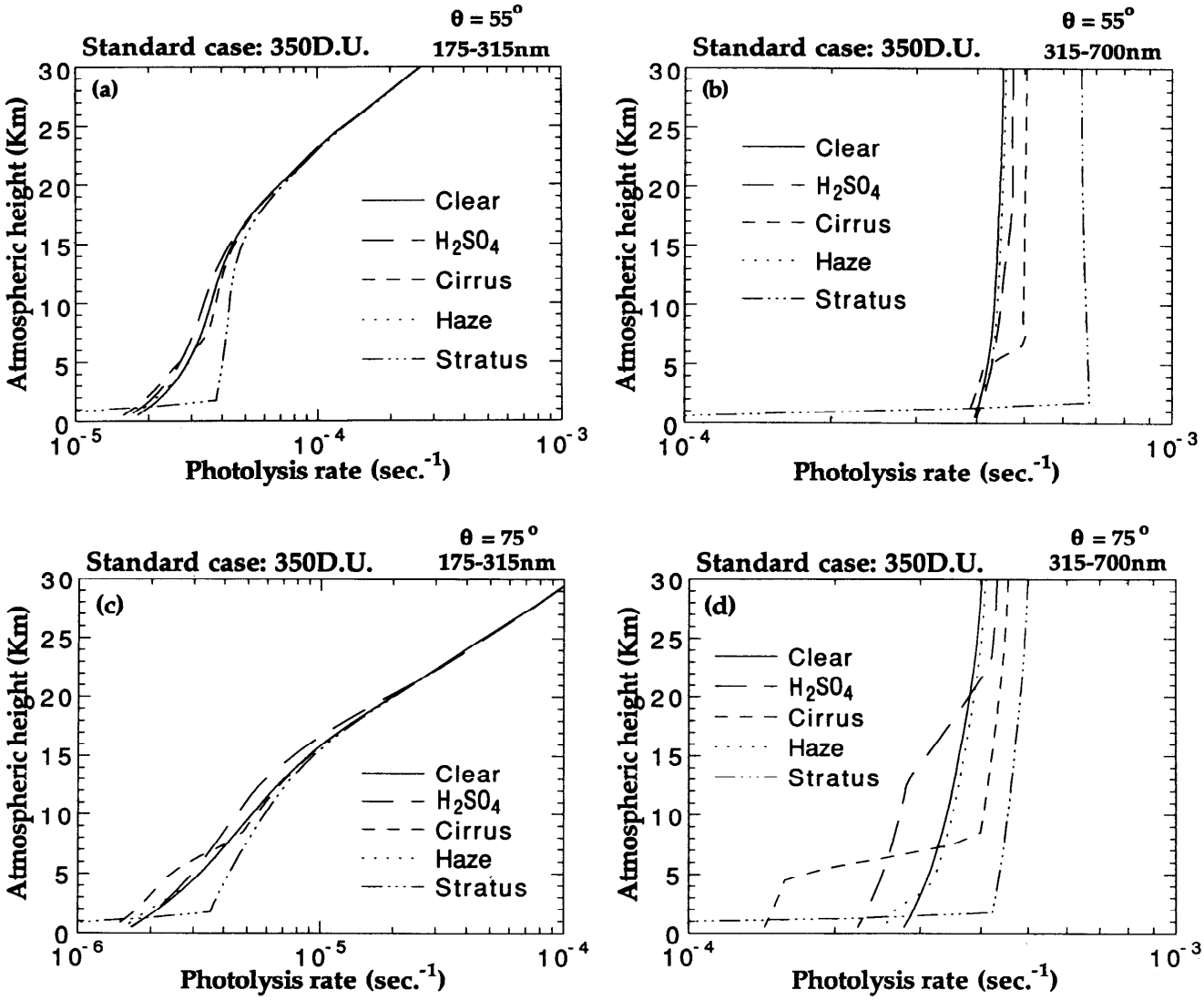

Fig. 7. Computed profiles of atmospheric photolysis rates (*a* - *d*) for the standard atmosphere of 350 DU ozone amount for two zenith angles and four spectral regions; and by different ozone scenarios (*e* - *f*) for arctic stratus cloud and 55° zenith angle; and (*g* - *h*) for stratospheric aerosol and 75° zenith angle.

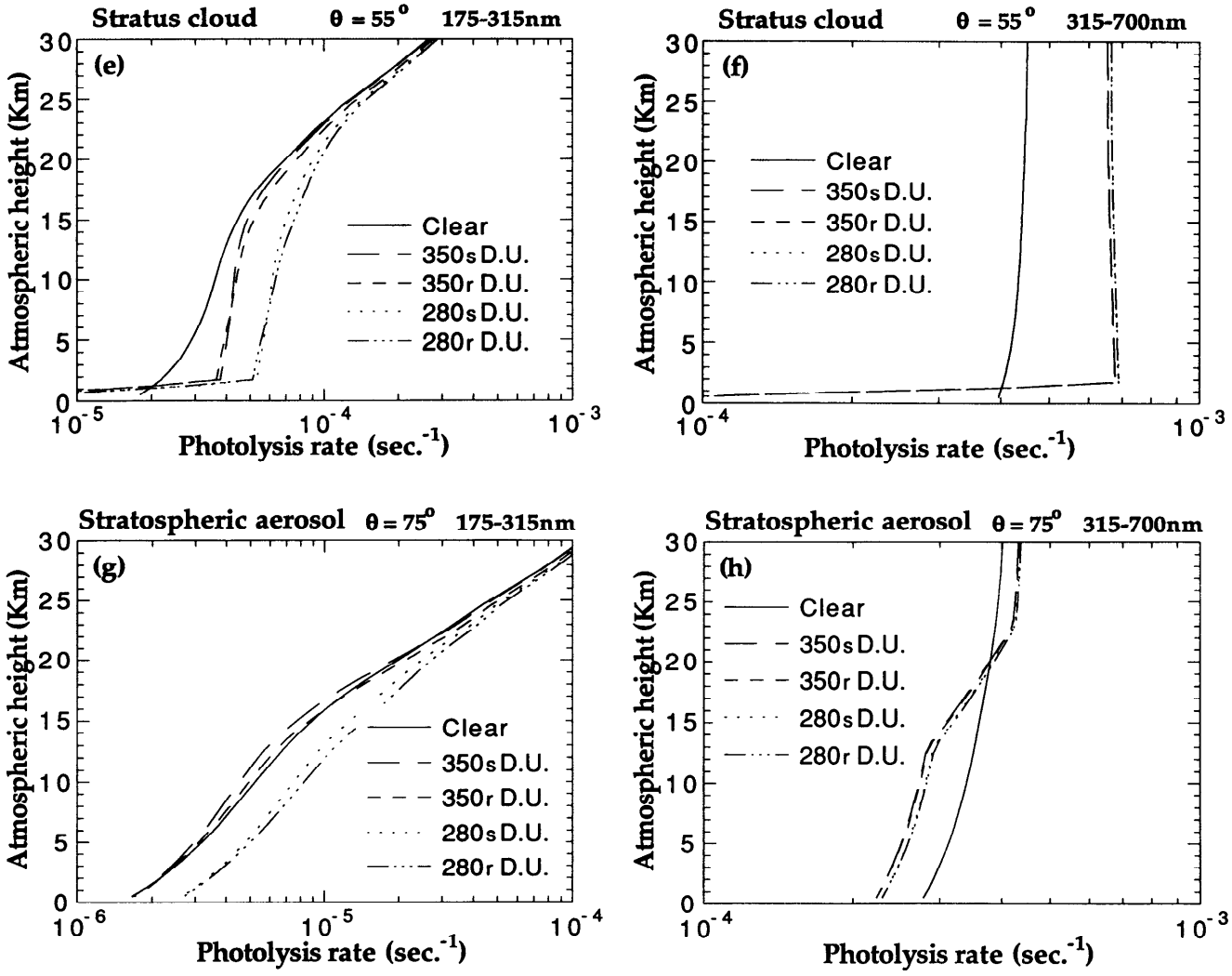

Fig. 7. (continued)

Figures 7*b* and 7*d* show corresponding results for the spectral interval between 315 nm and 700 nm. In this region of the spectrum the ozone absorption is relatively weak (cf. Figure 3); therefore multiple scattering by clouds play an important role. In the presence of arctic stratus clouds the photolysis rate may increase by 40%-70% throughout the entire atmosphere for a solar zenith angle of 55°. However, as the solar zenith angle increases the physical properties of the clouds become more important. The increased photon path length through the atmosphere may not only decrease the magnitude but also change the direction of the change (increase or decrease) of the photolysis rates below the clouds, depending on their scattering characteristics.

In Figures 7*e*-7*h*, we examine the impact of clouds on photolysis rates for the assumed ozone depletion/redistribution scenarios caused by stratus clouds and stratospheric aerosols to emphasize their different effects. Under the high sun (55°) and low-level stratus cloud conditions (Figures 7*e*-7*f*), the photolysis rates increase significantly with the ozone depletion for both spectral ranges (i.e., the production rates of both $O[^3P]$ and $O[^1D]$ are enhanced). As might be anticipated, for a redistribution of ozone from the stratosphere to the troposphere, the photolysis rate increases slightly in the stratosphere and decreases in the troposphere. However, when a high altitude cloud consisting of stratospheric aerosols is illuminated by low sun (75°), the resulting effects on the photolysis rates are as expected very different both in magnitude and structure from those of the stratus clouds (Figures 7*g* and 7*h*).

5. Summary and Conclusions

Penetration of UV radiation through the atmosphere is strongly influenced by atmospheric ozone and particulate matter, notably clouds and aerosols. Ozone absorbs strongly in the ultraviolet part of the spectrum and weakly in the visible. Particulate clouds interact significantly with solar radiation throughout the UV and visible region. This implies that the amount of UV and visible radiation available at any level in the atmosphere or at the surface is to a large extent determined by ozone abundance and cloud conditions. Therefore, quantities depending directly on the radiation field such as atmospheric warming and photolysis rates (and hence dynamics and chemistry) as well as the ultraviolet radiation reaching the biosphere (affecting human health and ecosystems on Earth), depend sensitively on a number of factors in the

Earth-atmosphere system including atmospheric composition and surface reflectivity. Yet the impact of particulate clouds on the radiation field constitutes one of the least understood elements of the system.

In this paper we have used a model of the arctic atmosphere, including cloud and aerosol properties constrained by available observations, in conjunction with a radiative transfer model to examine the combined effects of clouds and ozone on atmospheric warming/photolysis rates and the penetration of ultraviolet radiation into the biosphere. We have considered four types of particulate clouds prevalent in the summertime Arctic: stratospheric aerosol, cirrus clouds, tropospheric aerosol (arctic haze), and stratus clouds. Ozone depletion and alterations in the vertical distribution of ozone affect ultraviolet penetration and could have important ecological consequences. Such perturbations in ozone behavior could also contribute to climate change on a regional and/or global scale by modifying the atmospheric temperature structure and thereby the circulation. To study these effects, we have adopted a 20% ozone depletion scenario and examined the impact of a redistribution of ozone from the stratosphere to the troposphere.

The biological implications of our study may be summarized as follows: (1) stratus clouds provide a substantial shield from UV exposure; (2) stratospheric aerosols and tropospheric aerosols (arctic haze) have similar effects on the combined UVA and UVB exposure, but for low solar elevations stratospheric aerosols may lead to an increase in UV dose rate, while arctic haze results in a decrease; (3) a redistribution of ozone from the stratosphere to the troposphere tends to decrease UV exposure, except for low solar elevations where an increase may instead occur; and (4) the percent increase in UV dose rate per percent decrease in ozone abundance (radiation amplification factor) is largest (and tend to increase with solar zenith angle) for biological response heavily weighted towards UVB radiation (e.g., plant response), while biological effects with a significant response to UVA radiation (e.g., erythema) will have a smaller amplification factor that decreases with increasing solar zenith angle.

Atmospheric warming rates are affected as follows: (1) a 20% ozone depletion scenario and 55° solar zenith angle lead to about 0.4 K/d decrease of warming in the lower stratosphere, and redistribution in ozone to an increase of about 0.015 K/d in the upper troposphere; (2) a low-level stratus cloud may cause a large increase in radiative heating in the middle and upper stratosphere (about 0.8 K/d); (3) absorption of solar radiation in the lower stratosphere depends primarily on ozone content, but for the mid- and upper stratosphere, cirrus and stratus clouds lead to warming and stratospheric aerosols and arctic haze to cooling; (4) redistribution of ozone from the stratosphere to the troposphere results in enhanced tropospheric warming of a few hundredths K/d; and (5) perturbation in the absorption of solar radiation in the atmosphere is likely to be the consequence of an ozone depletion, because the resulting warming in the lower troposphere and cooling in the lower stratosphere can not be fully counteracted by the particulate clouds considered here. To what extent such perturbations will be amplified or damped by emission of terrestrial radiation remains to be investigated.

The effects of ozone depletion/redistribution and clouds on ozone photolysis rates may be summarized as follows: (1) for the photolysis leading to $O(^1D)$ production clouds have negligible impact at altitudes higher than 25 km because strong ozone absorption completely dominates for wavelengths less than 315 nm, but significant enhancements occur in the troposphere; (2) for photolysis leading to $O(^3P)$ production multiple scattering by clouds play an important role and the photolysis rate may increase by 50% or more throughout the atmosphere when stratus clouds are illuminated by high sun in the Arctic; (3) photolysis rates leading to both $O(^1D)$ and $O(^3P)$ production increase significantly with ozone depletion under high sun and low-level stratus cloud conditions.

Acknowledgments. One of us (S.C.T.) greatly appreciates the continued encouragement and support of this work by M. King and W. Wiscombe. This study was partially supported by the National Science Foundation through grants DPP 86-18706 and DPP 88-16298 and by NASA through grant NAGW-2165 to the University of Alaska.

REFERENCES

Blanchet, J.-P., and R. List, Estimation of optical properties of arctic haze using a numerical model, *Atmos. Ocean, 21*, 444-465, 1983.

Brasseur, G., and S. Solomon, *Aeronomy of the Middle Atmosphere*, D. Reidel, Hingham, Mass., 1984.

Bruhl, C., and P.J. Crutzen, On the disproportionate role of tropospheric ozone as a filter against solar UV-B radiation, *Geophys. Res. Lett., 16*, 703-706, 1989.

Brune, W.H., Ozone crisis: The case against chlorofluorocarbons, *Weatherwise, 43*, 136-143, 1990.

Chandrasekhar, S., *Radiative Transfer*, Dover, New York, 1960.

Chesters, D., and A.J. Krueger, A video atlas of TOMS ozone data, 1978-88, *Bull. Am. Meteorol. Soc., 70*, 1564-1569, 1989.

Dahlback, A., and K. Stamnes, A new spherical model for computing the radiation field available for photolysis and heating at twilight, *Planet. Space Sci., 39*, 671-683, 1991.

Dahlback, A., T. Henriksen, S.H.H. Larsen, and K. Stamnes, Biological UV-doses and the effect of an ozone layer depletion, *Photochem. Photobiol., 49*, 621-625, 1989.

Edwards, D.P., Solar heating by ozone in the tropical stratosphere, *Q. J. R. Meteorol. Soc., 108*, 253-262, 1982.

Evans, W.F.J., Ozone depletion in the Arctic vortex at Alert during February 1989, *Geophys. Res. Lett., 17*, 167-170, 1990.

Farman, J.C., B.G. Gardiner, and J.D. Shanklin, Large losses of total ozone in Antarctic reveal seasonal ClO_X/NO_X interaction, *Nature, 315*, 207-210, 1985.

Fels, S.B., J.D. Mahlman, M.D. Schwarzkopf, and R.W. Sinclair, Stratospheric sensitivity to perturbations in ozone and carbon dioxide: Radiative and dynamical response, *J. Atmos. Sci., 37*, 2265-2297, 1980.

Frederick, J.E., and H.E. Snell, Tropospheric influence on solar ultraviolet radiation: The role of clouds, *J. Clim., 3*, 373-381, 1990.

Frederick, J.E., H.E. Snell, and E.K. Haywood, Solar ultraviolet radiation at the earth's surface, *Photochem. Photobiol., 50*, 443-450, 1989.

Heintzenberg, J., Particle size distribution and optical properties of arctic haze, *Tellus, 32*, 251-260, 1980.

Henriksen, K., K. Stamnes, and P. Ostensen, Measurements of solar UV, visible and near IR irradiance at 78°N, *Atmos. Environ., 23*, 1573-1579, 1989.

Heymsfield, A.J., K.M. Miller, and J.D. Spinhirne, The October 27-28, 1986, FIRE cirrus case study: Cloud microstructure, *Mon. Weather Rev., 118*, 2313-2328, 1990.

Hofmann, D.J., T.L. Deshler, P. Aimedieu, W.A. Matthews, P.V. Johnston, Y. Kondo, W.R. Sheldon, G.J. Byrne, and J.R. Benbrook, Stratospheric clouds and ozone depletion in the Arctic during January 1989, *Nature, 340*, 117-121, 1989.

Kiehl, J.T., and B.A. Boville, The radiative-dynamical response of a stratospheric-tropospheric general circulation model to changes in ozone, *J. Atmos. Sci., 45*, 1798-1817, 1988.

King, M.D., Harshvardhan, and A. Arking, A model of the radiative properties of the El Chichon stratospheric aerosol layer, *J. Clim. Appl. Meteorol., 23*, 1121-1137, 1984.

Kondratyev, K.Y., Radiation in the *Atmosphere*, Academic, San Diego, Calif., 1969.

Lacis, A.A., and J.E. Hansen, A parameterization for the absorption of solar radiation in the earth's atmosphere, *J. Atmos. Sci., 31*, 118-133, 1974.

Lubin, D., J.E. Frederick, C.R. Booth, T. Lucas, and D. Neuschuler, Measurements of enhanced springtime ultraviolet radiation at Palmer station, Antarctica, *Geophys. Res. Lett., 16*, 783-785, 1989.

Luther, F.M., and R.J. Gelinas, Effect of molecular multiple scattering and surface albedo on atmospheric photodissociation rates, *J. Geophys. Res., 81*, 1125-1132, 1976.

Madronich, S., Photodissociation in the atmosphere; 1., Actinic flux and the effects of ground reflections and clouds, *J. Geophys. Res., 92*, 9740-9752, 1987.

McClatchey, R.A., R.W. Fenn, J.E.A. Selby, F.E. Volz, and J.S. Garing, Optical properties of the atmosphere, *AFCRL-72-0497, 108 pp.*, Air Force Cambridge Res. Lab., Bedford, Mass., 1972.

Nicolet, M., Solar spectral irradiances with their diversity between 120 and 900 nm, *Planet. Space Sci., 37*, 1249-1289, 1989.

Nicolet, M., R.R. Meier, and D.E. Andersons, Jr., Radiation field in the troposphere and stratosphere from 240 to 1000 nm, II., Numerical analysis, *Planet. Space Sci., 30*, 935-983, 1982.

Penner, J.E., and F.M. Luther, Effect of temperature feedback and hydrostatic adjustment in a stratospheric model, *J. Atmos. Sci., 38*, 446-453, 1981.

Proffitt, M.H., J.J. Margitan, K.K. Kelly, M. Loewenstein, J.R. Podolske, and K.R. Chan, Ozone loss in the Arctic polar vortex inferred from high-altitude air-craft measurements, *Nature, 347*, 31-36, 1990.

Shaw, G., Atmospheric turbidity in the polar regions, *J. Appl. Meteorol., 21*, 1080-1088, 1982.

Shettle, E.P., and A.E.S. Green, Multiple scattering calculation of the middle ultraviolet reaching the ground, *Appl. Opt., 13*, 1567-1581, 1974.

Solomon, S., The mystery of the antarctic ozone "hole", *Rev. Geophys., 26*, 131-148, 1988.

Spinhirne, J.D., and A.E.S. Green, Calculation of the relative influence of cloud layers on received ultraviolet and integrated solar radiation, *Atmos. Environ., 12*, 2449-2454, 1978.

Stackhouse, P.W., Jr., and G.L. Stephens, A theoretical and observational study of the radiative properties of cirrus: Results from FIRE 1986, *J. Atmos. Sci., 48*, 2044-2059, 1991.

Stamnes, K., The theory of multiple scattering of radiation in plane parallel atmospheres, *Rev. Geophys., 24*, 299-310, 1986.

Stamnes, K., and S.C. Tsay, Optimum spectral resolution for computing atmospheric heating and photodissociation rates, *Planet. Space Sci., 38*, 807-820, 1990.

Stamnes, K., S.C. Tsay, W. Wiscombe, and K. Jayaweera, Numerically stable algorithm for discrete-ordinate-method radiative transfer in multiple scattering and emitting layered media, *Appl. Opt., 27*, 2502-2509, 1988.

Stamnes, K., J. Slusser, and M. Bowen, Biologically effective ultraviolet radiation, total ozone abundance, and cloud optical depth at McMurdo station, Antarctica September 15 1988 through April 15 1989, *Geophys. Res. Lett., 17*, 2181-2184, 1990.

Stephens, G.L., Radiative transfer through arbitrarily shaped optical media, Part II; Group theory and simple closures, *J. Atmos. Sci., 45*, 1837-1848, 1988.

Stolarski, R.S., R.D. McPeters, J.R. Herman, and P. Bloomfield, Global ozone trends from TOMS, paper presented at Fall Meeting, AGU, San Francisco, Calif., Dec. 3-7, 1990.

Strobel, D.F., Parameterization of the atmospheric heating rate from 15 to 120 km due to O_2 and O_3 absorption of solar radiation, *J. Geophys. Res., 83*, 6225-6230, 1978.

Thompson, A.M., The effect of clouds on photolysis rates and ozone formation in the unpolluted troposphere, *J. Geophys. Res., 89*, 1341-1349, 1984.

Tsay, S.C., and K. Jayaweera, Physical characteristics of arctic stratus clouds, *J. Clim. Appl. Meteorol., 23*, 584-596, 1984.

Tsay, S.C., K. Stamnes, and K. Jayaweera, Radiative energy balance in the cloudy and hazy arctic, *J. Atmos. Sci., 46*, 1002-1018, 1989.

Tsay, S.C., K. Stamnes, and K. Jayaweera, Radiative transfer in planetary atmospheres: Development and verification of a unified model, *J. Quant. Spectrosc. Radiat. Transfer, 43*, 133-148, 1990.

World Meteorological Organization, Report of the International Ozone Trends Panel 1988, *Rep. 18*, vols. I and II, Geneva, 1988.

World Meteorological Organization, Scientific Assessment of Stratospheric Ozone: 1989, *Rep. 20*, vols. I and II, Geneva, 1989.

K. Stamnes, Geophysical Institute and Department of Physics, University of Alaska, Fairbanks, AK 99775.

S.-C. Tsay, Universities Space Research Association, NASA/Goddard Space Flight Center, Code 913, Greenbelt, MD 20771.

(Received January 16, 1991;
revised November 15, 1991;
accepted November 15, 1991.)